Phase-Sensitive Region-of-Interest Computed Tomography

Lina Felsner[1]([✉]), Martin Berger[3], Sebastian Kaeppler[1], Johannes Bopp[1],
Veronika Ludwig[2], Thomas Weber[2], Georg Pelzer[2], Thilo Michel[2],
Andreas Maier[1], Gisela Anton[2], and Christian Riess[1]

[1] Pattern Recognition Lab, Computer Science, University of Erlangen-Nürnberg,
Erlangen, Germany
lina.felsner@fau.de
[2] Erlangen Centre for Astroparticle Physics, University of Erlangen-Nürnberg,
Erlangen, Germany
[3] Siemens Healthcare GmbH, Erlangen, Germany

Abstract. X-Ray Phase-Contrast Imaging (PCI) yields absorption, differential phase, and dark-field images. Computed Tomography (CT) of grating-based PCI can in principle provide high-resolution soft-tissue contrast. Recently, grating-based PCI took several hurdles towards clinical implementation by addressing, for example, acquisition speed, high X-ray energies, and system vibrations. However, a critical impediment in all grating-based systems lies in limits that constrain the grating diameter to few centimeters.

In this work, we propose a system and a reconstruction algorithm to circumvent this constraint in a clinically compatible way. We propose to perform a phase-sensitive Region-of-Interest (ROI) CT within a full-field absorption CT. The biggest advantage of this approach is that it allows to correct for phase truncation artifacts, and to obtain quantitative phase values. Our method is robust, and shows high-quality results on simulated data and on a biological mouse sample. This work is a proof of concept showing the potential to use PCI in CT on large specimen, such as humans, in clinical applications.

1 Introduction

X-ray Phase-Contrast Imaging (PCI) is a novel imaging technique that can be implemented with an X-ray grating interferometer [1]. Such an interferometer provides an X-ray absorption image, and additionally a differential phase-contrast image and a dark-field image. X-ray absorption and phase encode material-specific parameters that are linked to the complex index of refraction n, given as $n = 1 - \delta + i \cdot \beta$. Here, δ relates to the phase shift and β to the attenuation. Since PCI yields high soft tissue contrast [2,3], it is particularly interesting to apply it in Computed Tomography (CT). Figure 1 shows example sinograms for the absorption and phase, and the associated tomographic reconstructions.
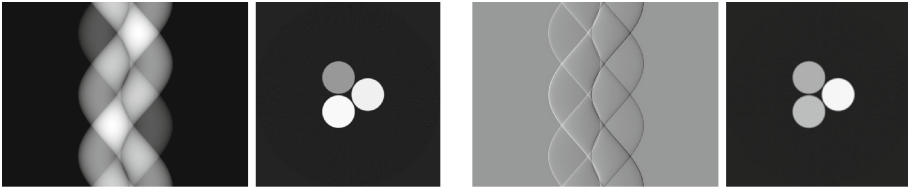
Fig. 1. Sinogram and reconstruction of the absorption (left) and differential phase images (right) of three cylinders with different materials at 82 keV. From the top in clockwise direction: water, PTFE and PVC.

It furthermore shows that their information is complementary, allowing for the distinction of different materials.

One key advantage of a grating-based interferometer is its compatibility with clinical X-ray equipment [1]. For clinical application, several practical challenges were recently addressed. Among these works are significant improvements in acquisition speed [4], higher X-ray energies to penetrate large bodies [5], and system vibrations [6].

However, one major obstacle to clinical implementation lies in the fact that it is not clear whether gratings with a diameter of more than a few centimeters can be integrated in a clinical CT system, due to increasing vibrations sensitivity, production cost and complexity for larger grating sizes. Such a small field of view is a major challenge for medical applications, since it only allows to reconstruct a small region of interest (ROI). This leads to difficult region localization and limited information on surrounding tissue. Furthermore, the object is typically larger than the field of view, which leads to truncation in the projection images.

Truncation is a substantial issue in the reconstruction of conventional projection images, leading to artifacts, such as cupping. Noo *et al.* showed that the reconstruction of a ROI from truncated differential images can be accurately obtained in certain cases [7]. Unfortunately, for the so-called interior problem, where the ROI is completely inside the object, there is no unique solution. Kudo *et al.* [8] found later, that the solution is unique if prior knowledge on the object is available in the form, that the object is known within a small region located inside the region of interest. For differential projection data, the interior problem can be approached iteratively [9,10]. However, these approaches are of limited practical use due to strong assumptions or high computational demand.

In this work, we propose a methodology for phase-sensitive region-of-interest imaging within a standard CT. The key idea is to solve the shortcomings of existing ROI imaging by complementing the small-area phase measurements with the full-field absorption signal, which is similar in spirit to the work by Kolditz *et al.* [11]. To this end, we propose to mount a grating-based system in the center of an absorption CT system. The truncated phase signal can be extrapolated beyond the grating limits using the full absorption information and the phase within the ROI. This mitigates the typical truncation artifacts, and

even provides quantitative phase information within the ROI, thereby paving the way towards phase CT in a clinical environment.
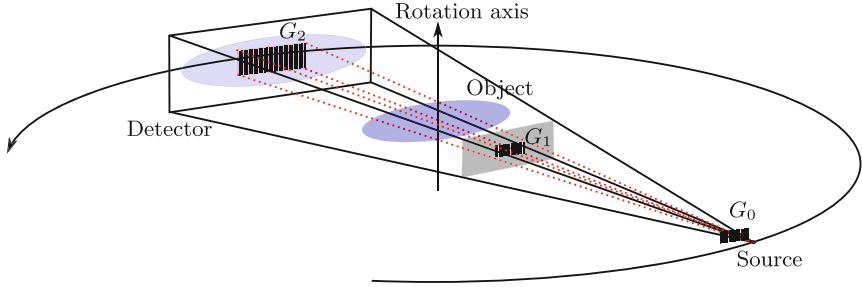
Fig. 2. Setup of the proposed imaging system.

2   Methods

The proposed method consists of a system and a reconstruction algorithm. We describe the system in Sect. 2.1 and the algorithm in Sect. 2.2.

2.1   Realization of the System

A grating-based (Talbot-Lau) interferometer consists of three gratings G_0, G_1, G_2 that are placed between X-ray tube and detector (see Fig. 2). G_0 is placed close to the source to ensure spatial coherence. G_1 is located in front of the object to imprint a periodical phase shift onto the wave front. G_2 is located in front of the detector to resolve sub-resolution wave modulations.

Recently, the implementation of an interferometer into a clinical-like C-arm setup was demonstrated [6]. We propose an embedding of the gratings in a clinical imaging system, such that the gratings cover only a region of interest. An attenuating collimator can be used for mounting the gratings, leading to less dose in the Peripheral Region (PR) outside of the gratings. PCI has a dose advantage compared to attenuation for high-resolution detectors [12], which suggests that it could also be advantageous to perform a high-resolution reconstruction in the ROI and reduce the resolution outside of the grating area to save dose. Figure 2 shows a sketch of the setup.

While the geometry of the full absorption image is a cone-beam, the smaller grating area exhibits approximately parallel beams, simplifying reconstruction. We apply a RamLak filter to the truncation-free absorption signal and a Hilbert filter to the phase-signal.

2.2   Truncation Correction

The pipeline of the proposed algorithm is shown in Fig. 3. We first perform a reconstruction of absorption and truncated phase, and segment the absorption
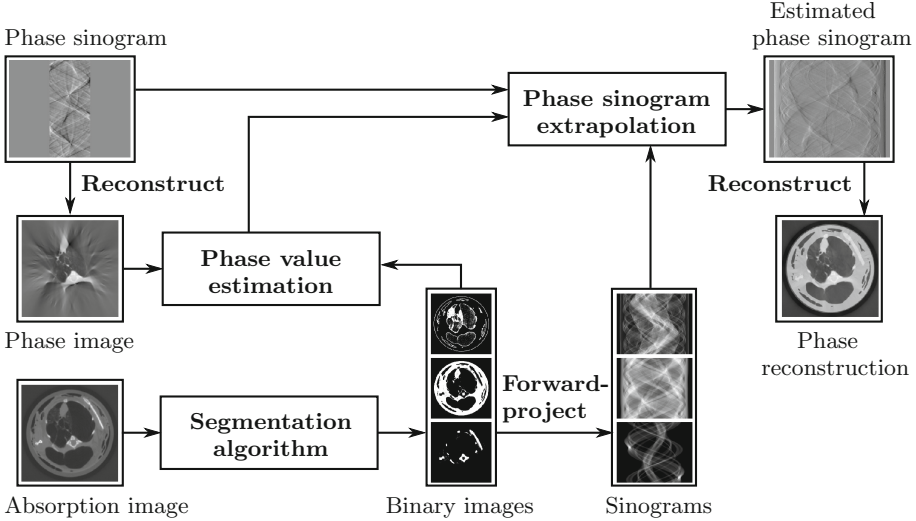
Fig. 3. Overview of the proposed method. A segmentation of the materials allows to obtain an estimate of their respective phase values. A non-truncated sinogram is extrapolated from the truncated sinogram and the extrapolated phase values.

into k materials. This allows to estimate the phase values per material within the ROI, and to extrapolate the phase values across the full area. Reconstructing then the phase from the estimated sinogram gives the non-truncated phase.

Segmentation Algorithm. The absorption signal is decomposed into k materials via segmentation. While in principle any algorithm could be used here, we fitted a Gaussian Mixture Model with k components to the histogram.

Phase Value Estimation. The truncated phase ROI is reconstructed. For each material, we estimate its phase value δ_k by computing the mean over its segmented pixels in the ROI. If a material is not contained in the ROI, we heuristically set it to the mean δ over the ROI. Since the estimated values will be differentiated in a later step, estimation bias is a minor concern.

**Phase Sinogram Extrapolation.** The phase shift ϕ is

$$\phi = \int \delta \, \mathrm{d}z = \sum_k \left(\delta_k \cdot \int_k \mathrm{d}z \right), \tag{1}$$

which can be split into k materials. The measured differential phase signal is

$$\varphi = \frac{\lambda \cdot d}{2\pi \cdot p_2} \frac{\partial \phi}{\partial x} = \frac{\lambda \cdot d}{2\pi \cdot p_2} \sum_k \left(\frac{\partial \, \delta_k \int_k \mathrm{d}z}{\partial x} \right), \tag{2}$$

consisting of sensitivity direction x, wavelength λ, $G_1 - G_2$ distance d, and the G_2 period p_2. The factor $(\lambda \cdot d)/(2\pi \cdot p_2)$ is the setup sensitivity, which is a

material-independent scaling factor and can therefore be ignored. Thus, we can obtain the sinogram of the differential phase by applying the derivative to the δ_k-weighted line integrals, given by the forward projections of the segmented materials. That way, the truncated phase sinogram is extrapolated with the missing sinogram information outside the ROI. The extrapolated phase together with the measured ROI allow for a quantitative phase reconstruction.
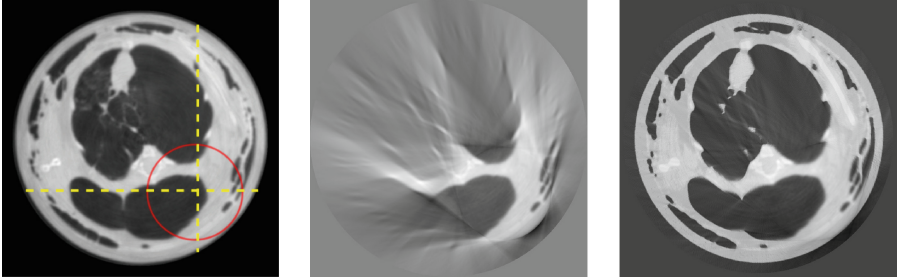
Fig. 4. Mouse sample. Left: ground truth with ROI (red) and line profile (yellow). Center: truncated phase reconstruction. Right: proposed phase reconstruction.
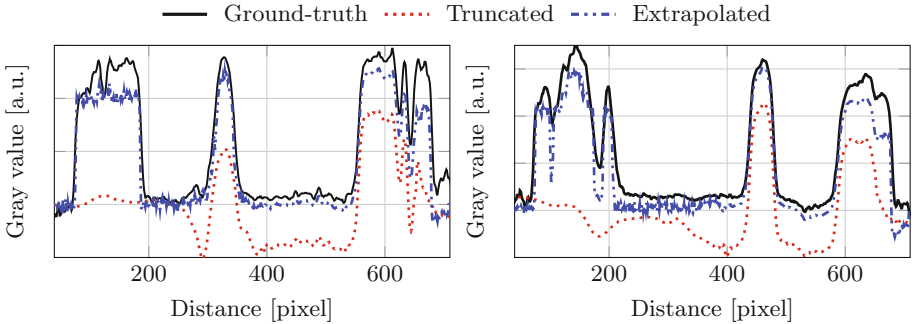
Fig. 5. Line plots of the mouse sample through the region of interest. Left: in horizontal direction; Right: in vertical direction.

3   Experiments

The proposed method is evaluated on a ground-truth reconstruction of the untruncated data after 3×3 pixel smoothing with a median filter. Line plots are obtained in horizontal and vertical direction through the center of the ROI. The quantitative metrics are the Root Mean Square Error (RMSE) and the Structural Similarity (SSIM) inside the ROI.

3.1   Biological Sample

We use a scan of a mouse [13] as biological sample with complex anatomical structures. The scan is manually truncated by cropping the ROI in the sinogram.

This allows us to compare the results to a full reconstruction. The acquisition setup consists of a tungsten anode X-ray tube at 60 kVp and a Varian PaxScan 2520D detector with 127 μm pixel pitch. The grating periods are 23.95 μm, 4.37 μm and 2.40 μm for G_0, G_1, and G_2, respectively. The $G_0 - G_1$ distance is 161.2 cm. Acquisition is done with 8 phase steps with exposures of 3.3 s each and a tube current of 30 mA. The image sequence contains 601 projection images over a full circle. We chose a ROI size of a third of the detector size.
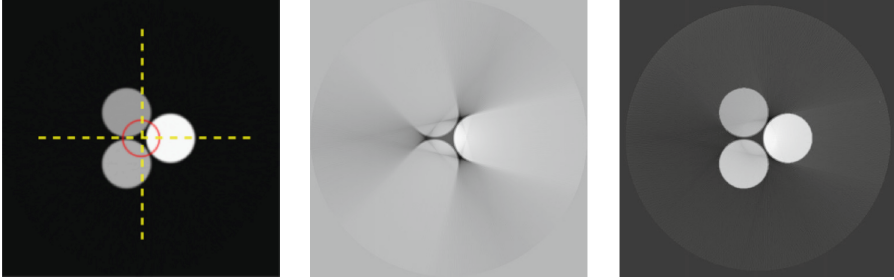
Fig. 6. Simulated sample. Left: ground truth with ROI (red) and line profile (yellow). Center: truncated phase reconstruction. Right: proposed phase reconstruction.
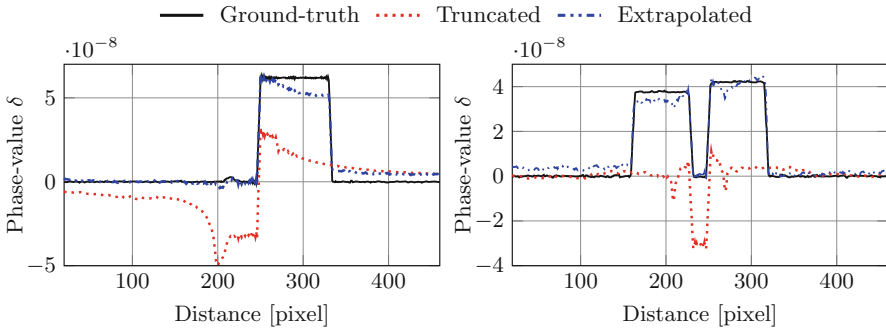
**Fig. 7.** Line plots on simulated sample in horizontal (left) and vertical direction (right).

We evaluate our method for nine different ROIs on the mouse, with k empirically set to 5. Our algorithm successfully reduces the truncation artifacts for all ROIs. Figure 4 shows example reconstructions of ground truth, truncated phase and estimated phase. The benefit of the truncation correction can be recognized both inside and outside of the ROI. The surrounding tissue of the ROI exhibits slightly sharpened edges due to the segmentation boundaries. The missing structure within the lung is a consequence of the rather simple segmentation. However, this has minimal impact on the quality of the phase information reconstructed within the ROI. The line plots after extrapolation in Fig. 5 are close to the ground truth. Table 1 depicts RMSE and SSIM relative to the ground truth. Our algorithm reduces the RMSE by more than 50%, and SSIM by 64%.

Table 1. Quality metrics with respect to the ground truth inside of the ROIs. Mean and standard deviation over 16 ROIs (simulated data) and 9 ROIs (mouse data).

	Simulation		Mouse	
	RMSE	SSIM	RMSE	SSIM
Truncated	$2.88E - 08 \pm 6.59E - 09$	0.46 ± 0.30	2.08 ± 0.27	0.30 ± 0.33
Estimated	$3.00E - 09 \pm 1.17E - 09$	0.99 ± 0.00	0.66 ± 0.14	0.94 ± 0.05

3.2   Quantitative Evaluation

The quantitative data was created by simulations using reported phase material values for water, polyvinylchlorid (PVC), and polytetrafluorethylen (PTFE) at 82 keV [14]. We used a parallel beam geometry and 360 projection images over a full circle. The size of the ROI is set to 1/8 of the detector width, k is set to 4.
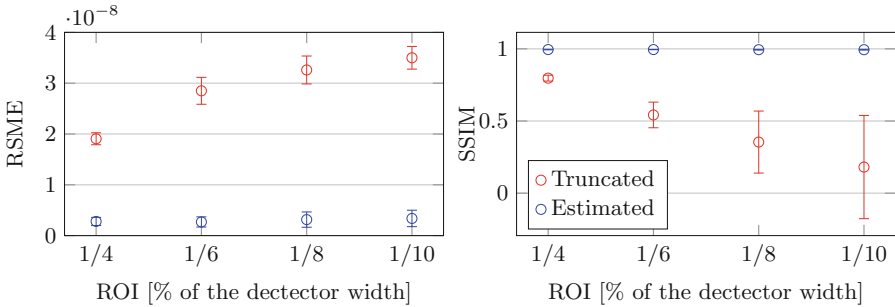
Fig. 8. Performance for simulated data at 82 keV, averaged over different ROI positions for 4 different ROI sizes. Red: truncated reconstruction. Blue: estimated reconstruction.

   The absorption and phase reconstructions are shown in Fig. 1. As PTFE and PVC have very similar absorption values, the segmentation erroneously labels them as identical materials. However, the proposed approach is robust to such a missegmentation, which can be recognized by the well distinguishable phase values of PVC and PTFE in Fig. 6. This is supported by the line plots in Fig. 7, where the correctness of the quantitative phase values can also be verified. The measurements in Table 1 support the visual impression, with an average improvement of over 50% for the SSIM and one magnitude decrease for the RMSE. Unfortunately, the phase value of PTFE in Fig. 7 (left) decreases slowly outside the ROI with increasing distance to the ROI.

   We also investigate the influence of the ROI size at four different locations, pushing the ROI away from the center. The mean error and standard deviation for RMSE and SSIM are visualized in Fig. 8. The quality of the truncated reconstruction is significantly decreased by a smaller ROI. Contrary, the proposed method is remarkably robust to changes in size and location of the ROI.

4   Conclusion

We propose a system and a method to perform quantitative ROI reconstruction of phase CT. The idea is to embed a grating interferometer into a standard CT, and to extrapolate the phase beyond the ROI with the absorption information to reduce truncation artifacts. Our results on quantitative data and a real biological sample are highly encouraging, and we believe that this is an important step towards using PCI on a clinical setup for larger samples.

Disclaimer. The concepts and information presented in this paper are based on research and are not commercially available.

References

1. Pfeiffer, F., Weitkamp, T., Bunk, O., David, C.: Phase retrieval and differential phase-contrast imaging with low-brilliance X-ray sources. Nat. Phys. **2**(4), 258 (2006)
2. Donath, T., et al.: Toward clinical X-ray phase-contrast CT: demonstration of enhanced soft-tissue contrast in human specimen. Inv. Rad. **45**(7), 445–452 (2010)
3. Koehler, T., et al.: Slit-scanning differential x-ray phase-contrast mammography: proof-of-concept experimental studies. Med. Phys. **42**(4), 1959–1965 (2015)
4. Bevins, N., Zambelli, J., Li, K., Qi, Z., Chen, G.H.: Multicontrast x-ray computed tomography imaging using Talbot-Lau interferometry without phase stepping. Med. Phys. **39**(1), 424–428 (2012)
5. Gromann, L.B., et al.: In-vivo x-ray dark-field chest radiography of a pig. Sci. Rep. **7**, 4807 (2017)
6. Horn, F., et al.: Implementation of a Talbot-Lau interferometer in a clinical-like c-arm setup: a feasibility study. Sci. Rep. **8**(1), 2325 (2018)
7. Noo, F., Clackdoyle, R., Pack, J.D.: A two-step hilbert transform method for 2D image reconstruction. Phys. Med. Biol. **49**(17), 3903 (2004)
8. Kudo, H., Courdurier, M., Noo, F., Defrise, M.: Tiny a priori knowledge solves the interior problem in computed tomography. Phys. Med. Biol. **53**(9), 2207 (2008)
9. Cong, W., Yang, J., Wang, G.: Differential phase-contrast interior tomography. Phys. Med. Biol. **57**(10), 2905 (2012)
10. Lauzier, P.T., Qi, Z., Zambelli, J., Bevins, N., Chen, G.H.: Interior tomography in x-ray differential phase contrast CT imaging. Phys. Med. Biol. **57**(9), N117 (2012)
11. Kolditz, D., Kyriakou, Y., Kalender, W.A.: Volume-of-interest (VOI) imaging in C-arm flat-detector CT for high image quality at reduced dose. Med. Phys. **37**(6), 2719–2730 (2010)
12. Raupach, R., Flohr, T.G.: Analytical evaluation of the signal and noise propagation in x-ray differential phase-contrast computed tomography. Phys. Med. Biol. **56**(7), 2219 (2011)
13. Weber, T., et al.: Investigation of the signature of lung tissue in x-ray grating-based phase-contrast imaging. arXiv (2012)
14. Willner, M., et al.: Quantitative X-ray phase-contrast computed tomography at 82 keV. Opt. Expr. **21**(4), 4155–4166 (2013)